Micron 40 (2009) 543–551

Contents lists available at ScienceDirect

Micron

journal homepage: www.elsevier.com/locate/micron

Two-dimensional quantitative mapping of arsenic in nanometer-scale silicon devices using STEM EELS–EDX spectroscopy

G. Servanton [a,b,*], R. Pantel [a], M. Juhel [a], F. Bertin [b]

[a] STMicroelectronics, 850 rue Jean Monnet, F-38926 Crolles, France
[b] CEA, LETI, MINATEC, 17 rue des Martyrs, F-38054 Grenoble, France

ARTICLE INFO

Article history:
Received 19 December 2008
Received in revised form 3 April 2009
Accepted 4 April 2009

Keywords:
STEM EELS–EDX
Silicon semiconductors
BiCMOS transistor
Arsenic dopant
EELS–EDX spectrum imaging

ABSTRACT

Field emission gun (FEG) nanoprobe scanning electron transmission microscopy (STEM) techniques coupled with energy dispersive X-ray (EDX) and electron energy loss spectroscopy (EELS) are evaluated for the detection of the *n*-type dopant arsenic, in silicon semiconductor devices with nanometer-scale. Optimization of the experimental procedure, data extraction and the signal-to-noise ratio versus electron dose, show that arsenic detection below 0.1% should be possible. STEM EDX and EELS spectrum profiles have been quantified and compared with secondary ion mass spectrometry (SIMS) analyses which show a good agreement. In addition, the arsenic doping level found inside large and small epitaxial devices have been compared using STEM EDX-EELS profiling. The average doping level is found to be similar but variable interface segregation has been observed. Finally, STEM EDX arsenic mapping acquired in a BiCMOS transistor cross-section shows strong heterogeneities and segregation in the epitaxially grown emitter part.

© 2009 Elsevier Ltd. All rights reserved.

1. Introduction

The detection and quantification of 2D dopant distributions with high spatial resolution are critical in order to understand the electrical performance of semiconductor devices. The dopant distribution is a key parameter which must be understood to optimize future device design through improved simulations. Nowadays, the required resolution to map dopants is in the nanometer-scale. Transmission electron microscopy (TEM) is in principle a very good candidate for dopant profiling if one considers its unsurpassed spatial resolution (atomic scale). However, to our knowledge, there is no publication showing the observation of dopants using classical bright field (BF) TEM imaging, with the exception of when coupled with chemical junction delineation (Siegelin et al., 2008). The reason is that the dopant contrast is very weak and masked by the dynamical diffraction effects due to strain, sample thickness variation and silicon crystal defects.

During the last decade, off-axis TEM electron holography has been used to record both phase and amplitude of transmitted electron images (Rau et al., 1999; Cooper et al., 2007). As the phase of an electron is sensitive to the electrostatic potential, the contrast from *p*–*n* junctions can be revealed using this method. Other methods that record the electrostatic potential use near field microscopy techniques such as Scanning Capacitance (SCM) and Scanning Spreading Resistance Microscopy (SSRM) (Eyben et al., 2007). Secondary Ion Mass Spectrometry (SIMS) is also a highly sensitive technique for the direct detection of dopants down to 10^{14} at. cm^{-3}. A recent and powerful technique for the detection of dopants is Atom Probe Tomography (APT) (Gault et al., 2006; Kelly and Miller, 2007; Thompson et al., 2007).

Regarding the literature, there are few publications on the subject of arsenic dopant distribution analysis by scanning transmission electron microscopy (STEM). Some authors use the Z contrast (Pei et al., 2008; Macaulay et al., 1993), which they evaluate to be limited to concentration above 1% (5×10^{20} at. cm^{-3}) (Parisini et al., 2008). Most of the papers concern Energy Dispersive X-ray spectroscopy (EDX) (Wang et al., 2001; Tsuneta et al., 2002; Topuria et al., 2001; Carpenter et al., 1999) and very few discuss Electron Energy Loss Spectroscopy (EELS) (Topuria et al., 2003). The sensitivity of these techniques was the limiting factor for the detection of low concentrations of dopants. However, analytical STEM hardware and methods have been improved during the last 10 years by the introduction of field emission guns, high brightness sources, probe correctors, and new spectrometer detectors. In addition the electrical and mechanical stability of the microscopes has been improved. Moreover, the latest generations of silicon devices have very high dopant concentrations which should prove to be easier to detect. Therefore, STEM EELS and EDX for dopant analysis distribution in highly doped *p*–*n* junctions should be re-evaluated due to the

* Corresponding author at: STMicroelectronics, 850 rue Jean Monnet, F-38926 Crolles, France. Tel.: +33 4 38 92 30 98.
E-mail address: germain.servanton@st.com (G. Servanton).

0968-4328/$ – see front matter © 2009 Elsevier Ltd. All rights reserved.
doi:10.1016/j.micron.2009.04.003

excellent spatial resolution available in modern TEM microscopes. In this paper, we have tried to optimize as much as possible the experimental parameters of STEM EELS and EDX analyses in order to push the sensitivity of the technique to be able to detect lower dopant concentrations. We will demonstrate the capability of STEM EELS and EDX to provide maps of dopants for real devices. We examine possible dopant concentration variations versus pattern dimension (for instance, size effect during epitaxy). Finally, STEM EDX mappings on Heterojunction Bipolar Transistors (HBTs) devices shows dopant heterogeneities and segregations that have been observed with nanometer-scale resolution and sensitivity below 0.1%, i.e., as low as 10^{19} at. cm^{-3}.

2. Experimental

The analytical STEM EELS and EDX experiments were performed using a FEG TECNAI F20 microscope with a Gatan energy filter GIF 200 and an EDAX detector. Experiments and processing were made using the EMISPEC TIA software and EELS quantification using Gatan Digital Micrograph software. The As doped Si samples were grown using CVD epitaxy (Borot et al., 2007). STEM EELS and EDX spectroscopy were used to investigate the As doped Si emitter part of SiGe-HBTs which fabrication process is explained elsewhere (Avenier et al., 2008). Samples were prepared using a gallium focused ion beam (FIB) in a dual beam FEI HELIOS with a final cleaning at low energy (5 keV). The lamella thickness were measured in EFTEM imaging mode using $t/\lambda = \ln(I_{Total}/I_{Elastic})$ knowing that the inelastic mean free path at 200 keV is about 150 nm in silicon (Delille et al., 1999). The probe current I(nA) was measured on the phosphorous screen in FEI TECNAI microscope: $I(\text{nA}) = (2.15\times(\text{emulsion}))/(\text{exposure time (s)})$.

For EELS, the FEG source was adjusted at 3800 V extraction voltage and gun lens 8. In these conditions (and this is valid for all FEI FEG microscopes: CM, TECNAI, TITAN), the EELS spectrum is clean above 1000 eV because the parasitic FEG gun lens electrons are displaced below that energy.

STEM EELS and EDX results on As doped emitter part of SiGe-HBT were compared to SIMS measurements performed on 300 μm $\times$ 300 μm test structures. SIMS experiments were achieved using a ADEPT 1010 model from Physical Electronics with 1.5 keV Cs^+ ion beam at 60° incidence angle.

3. STEM EELS/EDX spectrum background and signal-to-noise ratio

Here we analyze and compare the different characteristics of STEM EELS and EDX spectroscopy. The final objective is to optimize as much as possible the detection limit taking into account their respective properties. STEM EELS and EDX are two complementary techniques: in EELS, the direct ionization of core electron is detected and quantified in the spectrum, whereas, in EDX, the resulting electron–hole recombination leads to X-ray photons detected in the EDX spectrum. However, the two techniques differ from their respective detection geometry and detectors sensitivities. STEM EELS and EDX spectrum have also different characteristics if one considers the ionization edges signature, the energy resolution and the background levels.

3.1. STEM EELS/EDX spectrum background issue

First let us observe the typical EELS/EDX spectrum background (intensity level and energy dependence) and their respective signal and noise behaviour. Fig. 1 presents STEM EELS spectra obtained at 200 keV electron energy on 3.7% (18.5×10^{20} at. cm^{-3}) and 0.7% (3.5×10^{20} at. cm^{-3}) As doped Si samples for (0.8 nA $\times$ 10 s) electron dose. The EELS As-$L_{2,3}$ ionization threshold energy is 1323 eV and this edge is superimposed with a high background which must be subtracted by extrapolating a power law (E^{-r}). In Fig. 1(a), (Si–As 3.7%), the As-L edge is clearly detected. On the contrary, in Fig. 1(b), (Si–As 0.7%), the As-L edge is visible only if an accurate background extraction is carried out (see inset from Fig. 1(b)). Fig. 2 presents different EDX spectrum obtained at 120 keV on a Si–As doped (0.7% As) using variable exposure time and for 0.9 nA beam current. We only present the window around the As Kα peak. In Fig. 2(a), for a low dose (0.9 nA $\times$ 3 s), the spectrum intensity is very low, the background level is around one count and the As Kα signal is only few counts. The As Kα is visible but possibly below the detection limit due to the background noise. Increasing progressively the exposure time and dose in Fig. 2(b) (0.9 nA $\times$ 30 s) and Fig. 2(c) (0.9 nA $\times$ 120 s), the As Kα becomes more and more detectable. This clearly shows that the way to increase arsenic sensitivity and lower the detection limit is to increase the dose. Contrary to EELS, the background extraction is not really a problem since its level is flat and low. This is the reason why EDX experiments in this paper were done at 120 keV since for high dose at 200 keV, the electron beam will damage the sample over the relatively long acquisition times used here. The platinum peaks that are observed in the spectra from Fig. 2 come from the Pt FIB sample capping.

3.2. STEM EELS/EDX signal-to-noise ratio

The signal-to-noise ratio (S/N) versus electron doses for STEM EDX (120 keV) and STEM EELS (200 keV) has been assessed for the

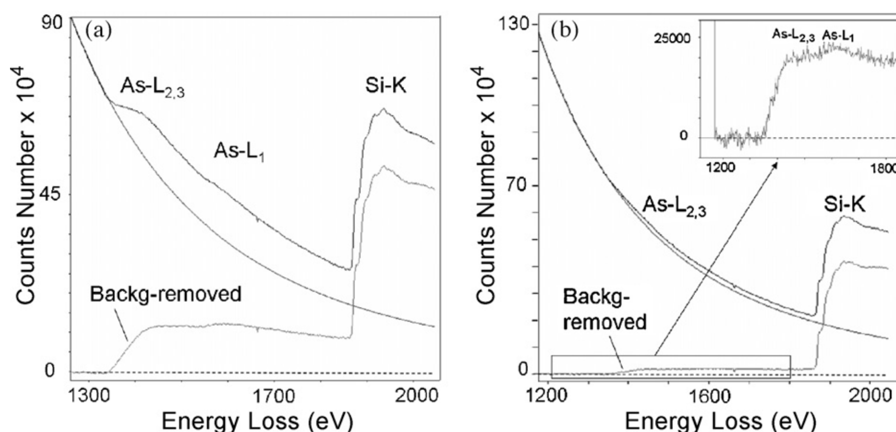

Fig. 1. 200 keV As-$L_{2,3}$ EELS spectrum and background removed from (a) 3.7% (18.5×10^{20} at. cm^{-3}) As doped Si layer, (b) 0.7% (3.5×10^{20} at. cm^{-3}) As doped Si layer. The inset is a zoom on the As-$L_{2,3}$ peak.

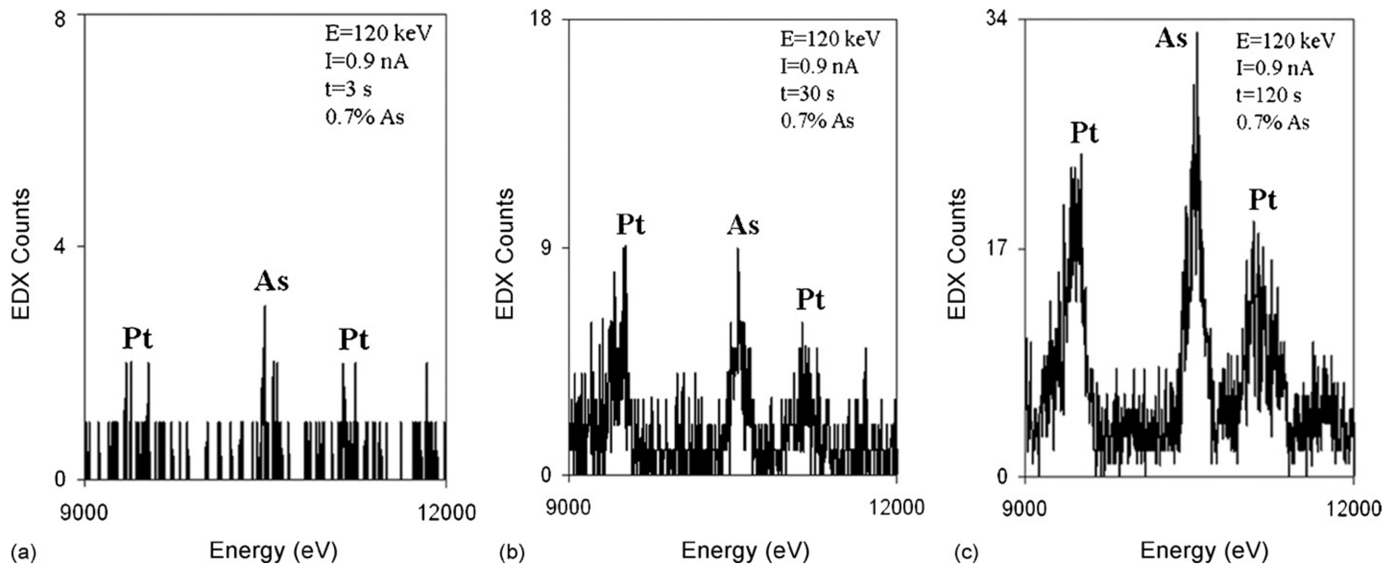

Fig. 2. (a) EDX spectra obtained at 120 keV on a 0.7% As doped Si for different increasing electron doses (a) (0.9 nA × 3 s), (b) (0.9 nA × 30 s), (c) (0.9 nA × 120 s).

Fig. 3. (a) STEM dark field Z contrast image of a 50 nm 3.7% (18.5×10^{20} at. cm^{-3}) As doped Si epitaxial layer. The line scan profile is indicated by the white arrow. (b) and (c) EDX As Kα and EELS As-L intensity line profiles performed on a 3.7% As doped Si layer with (0.9 nA × 3 s) and (0.3 nA × 3 s) doses, respectively. The signal and noise definitions are explained in (b) and (c).

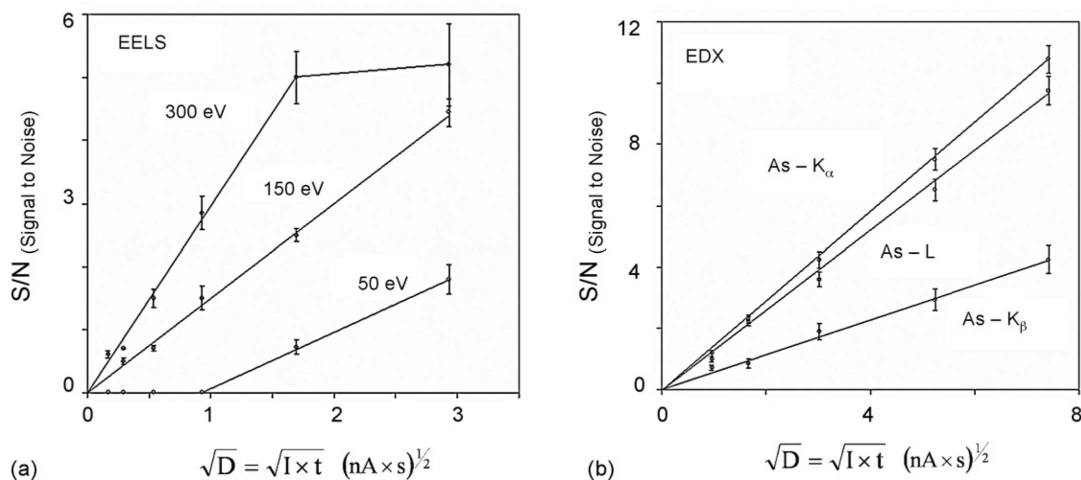

Fig. 4. (a) 200 keV STEM EELS signal-to-noise ratio versus $\sqrt{D}$ acquired on a 0.7% (3.5×10^{20} at. cm^{-3}) As doped Si for 300, 150 and 50 eV background and signal extraction energy windows. (b) 120 keV STEM EDX S/N versus the dose acquired on a 0.7% (3.5×10^{20} at. cm^{-3}) As doped Si for the As Kα, Kβ and As-L peaks.

same sample. Fig. 3 shows examples of STEM EDX and EELS line profiles and the method to measure the signal and noise on such profiles is indicated. Fig. 3(a) presents a 50 nm 3.7% As doped Si observed in STEM Z contrast mode; the arrow indicates the place of the line scan profile. Fig. 3(b) and (c) present the STEM EDX As Kα and EELS As-L intensity profiles obtained for (0.9 nA × 3 s)/pixel and (0.3 nA × 3 s)/pixel, respectively. In Fig. 3(b) and (c), the definitions of noise (N) and signal (S) measurements are shown. The total noise (N) is assumed to be the addition of As signal noise (N_S) plus Si background noise (N_{Bkg}) and the signal-to-noise S/N is calculated:

$$\frac{S}{N} = \frac{S}{N_{Bkg} + N_S}$$

In these profiles and more generally for dopant analysis, it is important to acquire enough data points inside the pure silicon in order to calibrate the As signal, where the averaged arsenic signal is S = 0. This will improve the EDX-EELS background extraction and will give a reliable zero reference for arsenic quantification.

Fig. 4(a) presents 200 keV EELS S/N measurements versus $\sqrt{D} = \sqrt{I \times t}$ (D is the dose, I the beam current in nA and t the exposure time in s) for the extraction of three energy windows (50, 150 and 300 eV, where in each case the width of the background window is the same as the signal window). The electron doses range from (0.3 nA × 0.1 s) to (0.3 nA × 30 s). The STEM EELS signal-to-noise ratio is linear with respect to $\sqrt{D}$, which will be expected from statistics. This indicates that EELS signal acquisition and signal extraction are of high quality, with the exception of the narrow 50 eV window. STEM EELS appears to be a very accurate spectroscopy mode for low electron doses (short exposure time) since the As-L edge signal-to-noise ratio rapidly reaches high values (~5) for doses as low as (0.3 nA × 10 s). Since the EELS S/N is higher than 5 in a 0.7% As doped Si sample, the arsenic detection limit is about 0.2% (10^{20} at. cm^{-3}). The reason why in Fig. 4(a) the signal-to-noise ratio seems to saturate for $\sqrt{D} > 1.7$ is possibly due to radiation damages and in this case a too large integration window (300 eV) is no more optimum.

STEM EDX spectrum profiles were acquired at 120 keV on the same 0.7% As doped Si specimen for doses ranging from (0.9 nA × 1 s) to (0.9 nA × 60 s). As Kα, Kβ and As-L peaks intensities are integrated over [10.36, 10.76 keV], [11.55, 12.00 keV] and [1.23, 1.38 keV] energy windows, respectively. Fig. 4(b) presents the EDX S/N experimental results versus $\sqrt{D}$ for the As Kα, Kβ and As-L peaks. The improved signal-to-noise ratio is obtained for the As Kα. The As-L peak is intrinsically more intense but at its energy (around 1 keV), the Bremsstrahlung background is high. The signal-to-noise ratio increases linearly versus $\sqrt{D}$ up to doses as high as (0.9 nA × 60 s). On this 0.7% As sample, the As Kα signal-to-noise ratio is about eleven for a dose (0.9 nA × 60 s). This suggests that the detection limit is in this case better than 0.1%. Since no saturation occurs at 120 keV, the dose can still be increased using active drift corrected STEM line profile analysis.

4. STEM EELS/EDX quantification method

As a first step, we have calibrated both the STEM EELS and EDX using a very well known Si(Ge) reference sample. We used different quantification methods. First, since we have a very good Si(Ge) reference specimen calibrated using XRD and SIMS, we adjusted EELS and EDX from the Si(Ge) system (transitions Si-K and Ge-L for EELS and Si-K Ge-K for EDX). We then considered that the Si(As) system is nearly equivalent to Si(Ge) (i.e., we used the same cross-section and K-factor for As and Ge atoms). Additionally, Si(Ge) reference and Si(As) buried layer were also quantified in EELS spectroscopy by Digital Micrograph (DM) Gatan software with Hartree–Slater cross-sections. A comparison between Si(Ge) and Si(As) quantification using K-factors and DM software are indicated in Table 1.

The very accurate Si(As) quantification confirms that As and Ge have similar cross-sections.

The atomic concentration ratio between two elements A and B is related to the measured intensities ratio (I_A, I_B) by the Cliff–Lorimer equation (Cliff and Lorimer, 1975):

$$\frac{C_A}{C_B} = k_{AB}\frac{I_A}{I_B}.$$

In our case, A will be either arsenic or germanium and B is silicon, k_{AB} is the sensibility factor which depends on the acceleration voltage, STEM EELS and EDX experimental parameters

Table 1
STEM EELS As quantifications using K-factor (with a Ge reference sample) and Hartree–Slater cross-sections from DM Gatan software.

Quantification	Sample		
	Si(Ge)3.9%	Si(As)3.7%	Si(As)0.7%
K-factor	3.9%$_{ref}$	3.75%	0.75%
DM Gatan	3.7%	3.85%	0.8%

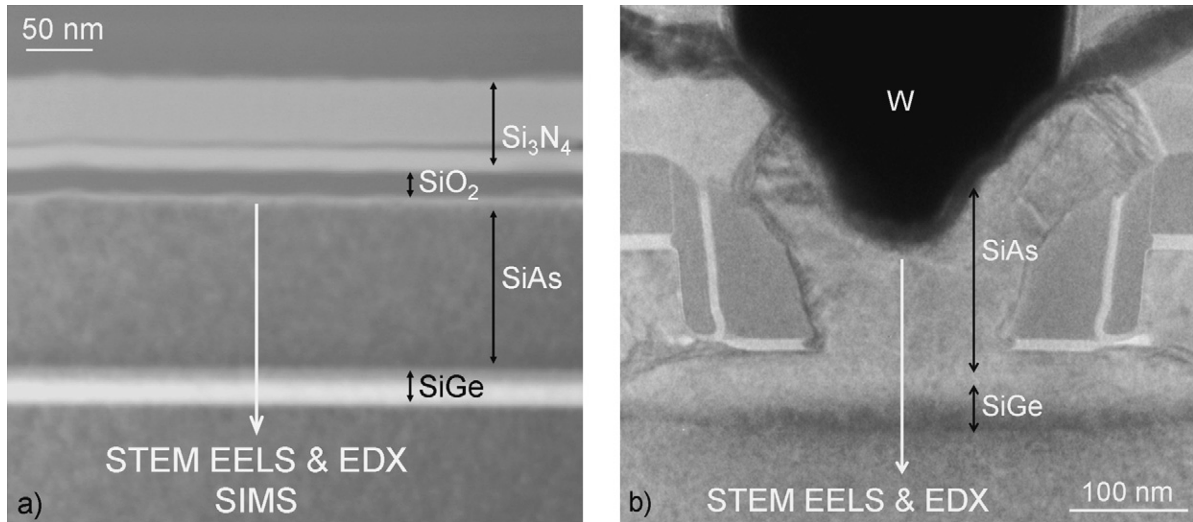

Fig. 5. (a) STEM image from a lamella cross-section extracted in the SIMS test structure with the stack under analysis. The positions of the STEM EELS and EDX line profile are indicated by the white arrow. (b) TEM image of a HBT with the same stack (Si(Ge)/Si(As) epitaxy) than the SIMS test structure. The position of the STEM EELS and EDX line profile are indicated by the white arrow.

and data processing (i.e., the EELS energy integration windows). The thicknesses of the specimens were always in the range of 150 ± 50 nm and the sensitivity factor was considered stable for this thickness range. For STEM EDX, we assumed the specimens to be thin enough to ignore any absorption or fluorescence phenomena. We found the 120 keV STEM EDX sensibility $k_{Ge} \equiv k_{As}$ to be equal to 1.1 for Ge-K and Si-K. In the case of 200 keV STEM EELS analysis, we used a 50 μm C2, a STEM spot size 3 and a camera length 30 mm. Ge-L and Si-L integration windows widths are chosen to be 300 and 170 eV, respectively and, in this case, EELS sensibility factor is found to be around 13.

5. Experimental applications in silicon devices

For a long time it has been suspected that during processing, the size of features will influence the actual dopant concentrations in the devices, especially for epitaxy. These effects could not be experimentally evaluated up to now since no accurate dopant analysis and quantification techniques with nm-resolution existed. Here we reveal that it is now possible to measure the dopant concentration as a function of the structure size. The STEM EELS and EDX were calibrated by comparing the results with SIMS analysis obtained on a large As doped Si epitaxial structure (300 μm × 300 μm). EELS and EDX were then performed on actual BiCMOS transistors.

5.1. EELS/EDX quantification comparison with SIMS in large structure

Fig. 5(a) presents a STEM image from the lamella cross-section extracted from a SIMS test structure integrating a Si/Si(Ge)/Si(As) stack. Fig. 5(b) shows the TEM image of a BiCMOS transistor using an identical stack which had been epitaxially grown on the same wafer. Both stacks comprise from bottom to top, a Si substrate, a 20 nm Si(Ge) layer, followed by a 10 nm undoped Si layer and finally a 200 nm Si(As) layer. These have been examined for two different epitaxial processes. In Process 1, the substrate surface was saturated with arsenic (AsH_3 gas without SiH_4) before starting the Si(As) epitaxy. Then, the film was grown with AsH_3 and SiH_4 constant fluxes at 650 °C. In Process 2, AsH_3 and SiH_4 gases were introduced at the same time and kept at constant flow (i.e., the arsenic concentration in silicon was gradually increased by progressive surface saturation). First STEM EELS and EDX profiles

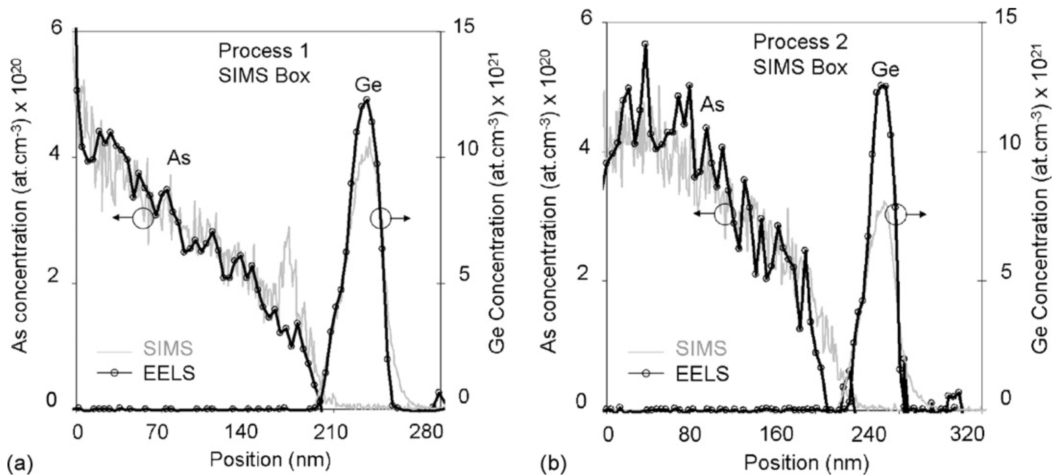

Fig. 6. (a) and (b) SIMS profiles (grey lines) performed in the SIMS test structure (300 μm × 300 μm) for Processes 1 and 2. 200 keV STEM EELS profiles (black lines) performed in the same test structure.

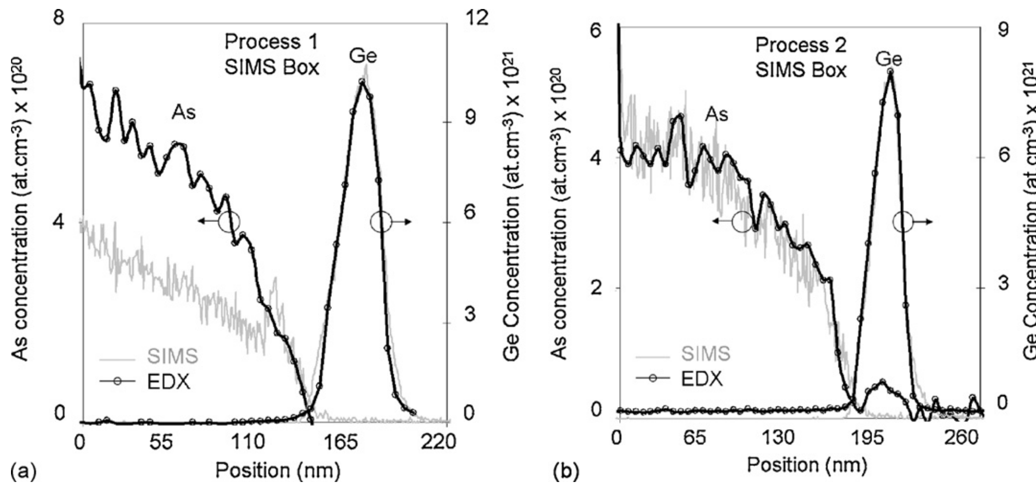

Fig. 7. (a) and (b) SIMS profiles (grey lines) performed in the SIMS test structure (300 μm × 300 μm) for Processes 1 and 2. 120 keV STEM EDX profiles (black lines) performed in the same test structure.

were acquired on TEM lamellae prepared from the test structures for each of the differently processed wafers in order to compare the results with SIMS.

In Fig. 6(a) and (b), the SIMS profiles are indicated by grey lines for Processes 1 and 2. These profiles are then compared in Fig. 6(b) with 200 keV STEM EELS line scans indicated using black lines. The STEM EELS profiles, quantified using the method presented previously, fit very well with the SIMS profiles. These results suggest that the quantification method is accurate. Moreover, despite that the analyzed area is in nanometer range, the STEM EELS is sensitive enough and not too noisy to be compared with SIMS. However, we should note that for Process 1 shown in Fig. 6(a), the SIMS profile shows a peak near the Si undoped/As doped interface. This peak is not observed in the STEM EELS profile. This will be discussed later. The STEM EELS profile also seems to have a better resolution which is revealed by a sharper Ge peak. These results are promising for arsenic detection and quantification on small devices. This shows that STEM EELS could be used to determine doping uniformity with nm-resolution.

In Fig. 7(a) and (b), the SIMS profiles acquired for Processes 1 and 2 are shown again. These profiles are compared in Fig. 7(a) and (b) to the 120 keV STEM EDX profiles indicated by the black lines. The general arsenic gradient trend is reproduced in the EDX spectrum profiles but the quantification, in particular for Process 1, is not in good agreement with SIMS. The profiles were acquired three times from the same location and we have observed for EDX quantification important fluctuations and errors ±30%. This point is discussed later in the general discussion. The same conclusion for EELS concerns also the fact that for Process 1, the interface peak is not observed in EDX. This point will also be discussed later.

5.2. Comparison of arsenic doping in large and small devices (BiCMOS transistor)

Fig. 8(a) and (b) presents a comparative study of 200 keV STEM EELS profiles acquired from large test structures (grey lines) and in BiCMOS transistors (black lines) for Processes 1 and 2. In the BiCMOS transistor, the Si(As) layer is thinner (100 nm) than in the SIMS box structure due to a different process (etching and lithography). This is the reason why As profiles are shorter in Fig. 8. For Processes 1 and 2, the quantification of the STEM EELS in the test structure and in the BiCMOS fit well. No dimensional effects during epitaxial layer growth have been detected. Nevertheless the STEM EELS profile obtained on the wafer with Process 1 clearly shows an As segregation at the intrinsic layer/Si(As) interface.

Fig. 9(a) and (b) shows 120 keV STEM EDX profiles acquired on test structure (grey lines) and BiCMOS (black lines) for Processes 1 and 2. As explained on Fig. 7(a) and (b), the STEM EDX quantification is somehow unstable (see Section 6). This is probably the reason why the profiles differ from the acquisition

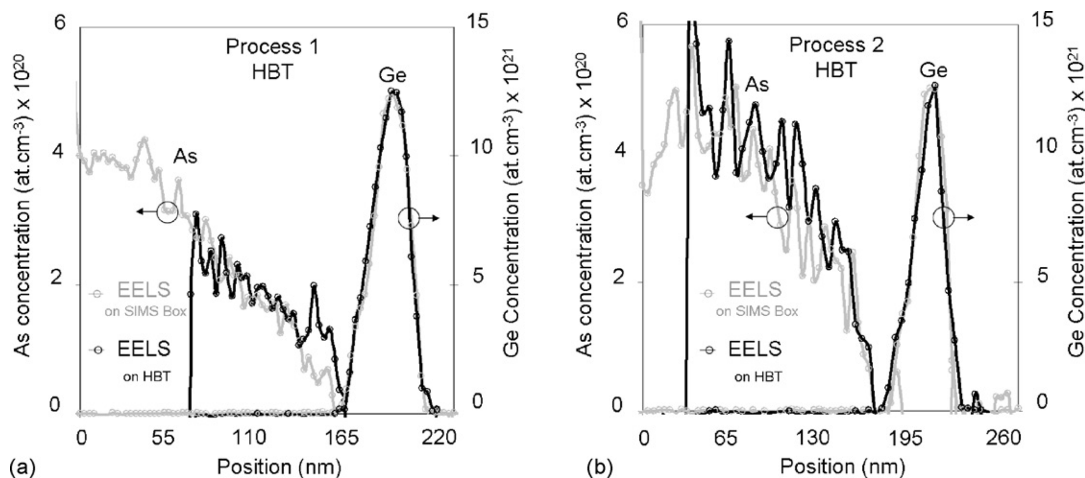

Fig. 8. (a) and (b) 200 keV STEM EELS comparative study between profiles acquired in test structures (grey lines) and in HBTs (black lines) for Processes 1 and 2.

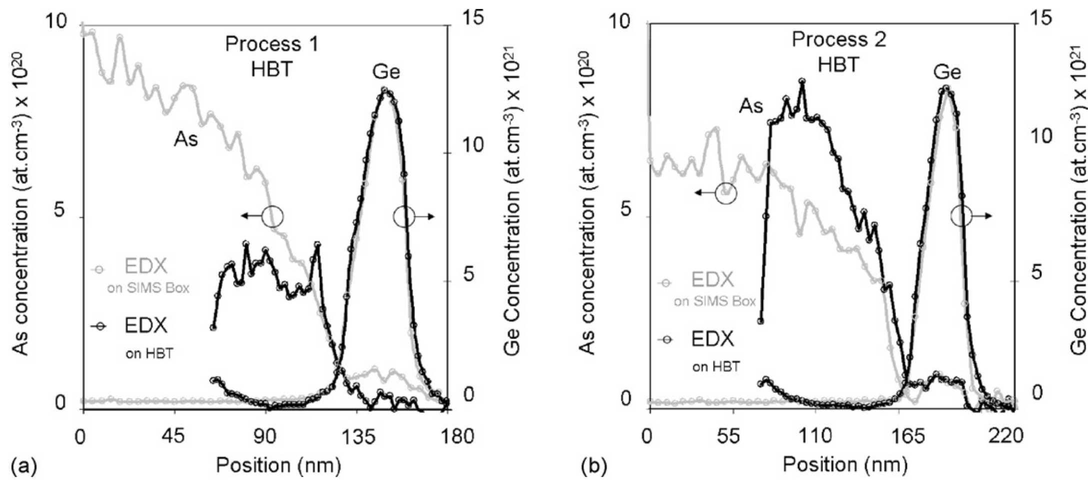

Fig. 9. (a) and (b) 120 keV STEM EDX profiles acquired on test structure (grey lines) and HBTs (black lines) for Processes 1 and 2.

in the large structure. Nevertheless, the shape of the profile and the concentration range are still coherent with the expected values. The arsenic segregation at bottom interface is also observed for Process 1.

To summarize, we do not see a global arsenic concentration variation between large and small devices. On the contrary, for Process 1, concerning the bottom interface segregation arsenic peak, the EDX and EELS profiles show a difference between the large and small devices. This suggests that the first AsH_3 flash used in Process 1 will saturate more efficiently the initial interface inside small devices than in large devices.

5.3. Control of the arsenic dopant distribution homogeneity in nano-devices

Dopant heterogeneities, such as segregation, in the emitter part of a bipolar transistor are undesirable since they can drastically affect their performance. Fig. 10(a) and (b) shows a TEM image and 120 keV STEM EDX profile acquired vertically across the emitter and base of a HBT. For this STEM EDX profile, the dose/pixels is (1 nA $\times$ 30 s). In the bottom part of the emitter, the As concentration is about 0.3% (1.5 $\times$ 10^{20} at. cm^{-3}). A strong segregation with a 1% (5 $\times$ 10^{20} at. cm^{-3}) As peak is recorded at the epitaxial interface (point 2 in Fig. 10). This arsenic heterogeneity was not expected and can lead to bad performance of the device. In order to get a better and complete knowledge about arsenic doping heterogeneities distribution in the BiCMOS transistors, we have also acquired 120 keV STEM EDX maps on the emitter part of another BiCMOS.

Fig. 11(a) shows the TEM image of this BiCMOS, showing polysilicon grain boundaries in the emitter. Fig. 11(b) presents a 120 keV STEM EDX map acquired in the center of the emitter for a resolution of 100 $\times$ 100 pixels (spectrum). The electron dose used in this experiment was (1 nA $\times$ 5 s) per pixel for a total of 14 h acquired in four runs and recombined as a mosaic map. Arsenic distribution heterogeneities are clearly detected in particular segregation at the grain boundaries and at the spacer (Si_3N_4) edges. Furthermore, a depleted As region is shown at the bottom of emitter, just above the intrinsic layer and the Si(Ge) base. The observation of the arsenic map suggests that at the bottom of the emitter during the beginning of the Si(As) epitaxy growth, the arsenic does not incorporate well in the bulk. The As was then pushed to the top emitter because the Si surface gradually saturates with a high As concentration during growth. Finally, the top of the grain has a high As concentration. Also, the As accumulates on the spacers giving a higher concentration in this area. The profiles extracted from the emitter/base region are very different at the center and edge of the BiCMOS device. This can lead to electron injection behaviour variation from edge to center. Those results are of important to better understand the electrical performance and can be used for improving devices simulations.

In order to quantify the arsenic heterogeneities in the complete emitter and at the grain boundaries, 120 keV STEM EDX profiles

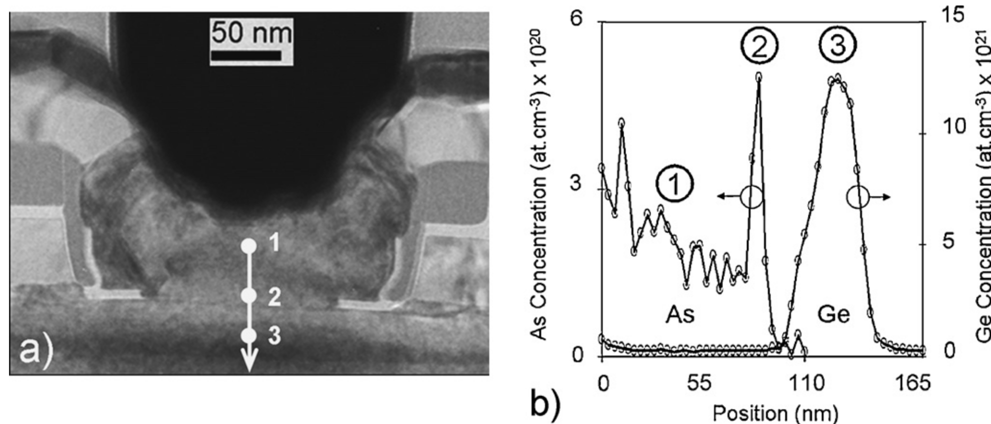

Fig. 10. (a) TEM image of a HBT region of interest consisting of an As gradient in the emitter part and Ge in the base. The white arrow indicates the EDX profile and positions 1, 2 and 3 are reported on the following graph. (b) 120 keV STEM EDX profile vertically acquired across the emitter (point 1) and base (point 3) of a HBT. An As segregation is revealed by the EDX profile at the interface with the Ge base (point 2).

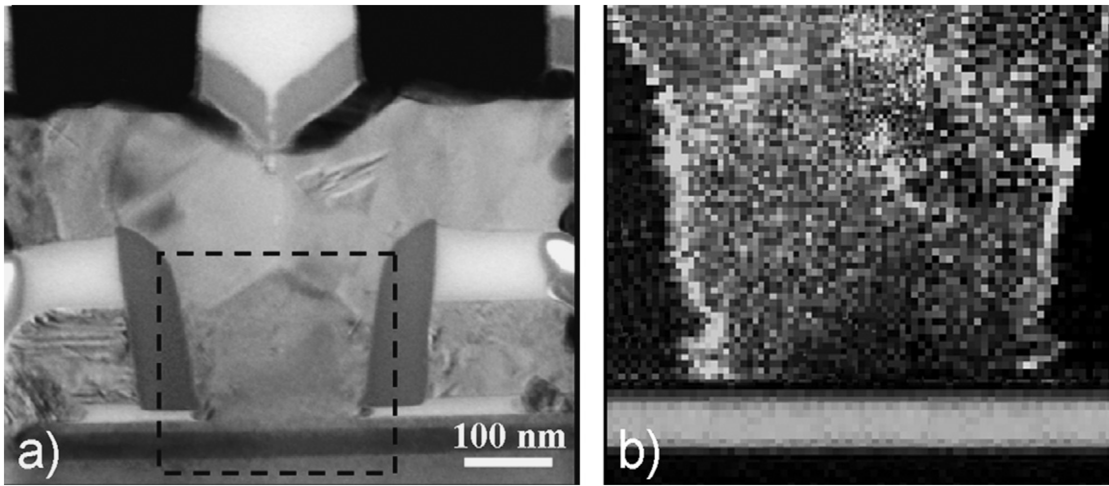

Fig. 11. (a) TEM image of another HBT showing polysilicon grain boundaries in the emitter. The dashed square is the region of interest where an As EDX mapping is performed. (b) 120 keV STEM EDX mapping acquired in the center of the emitter part of a HBT with (1 nA × 5 s/pixels) dose for around 100 × 100 pixels. The As segregation is clearly revealed at the spacer edges and at the polysilicon grain boundaries. An As depleted region is also visible at the interface with the base.

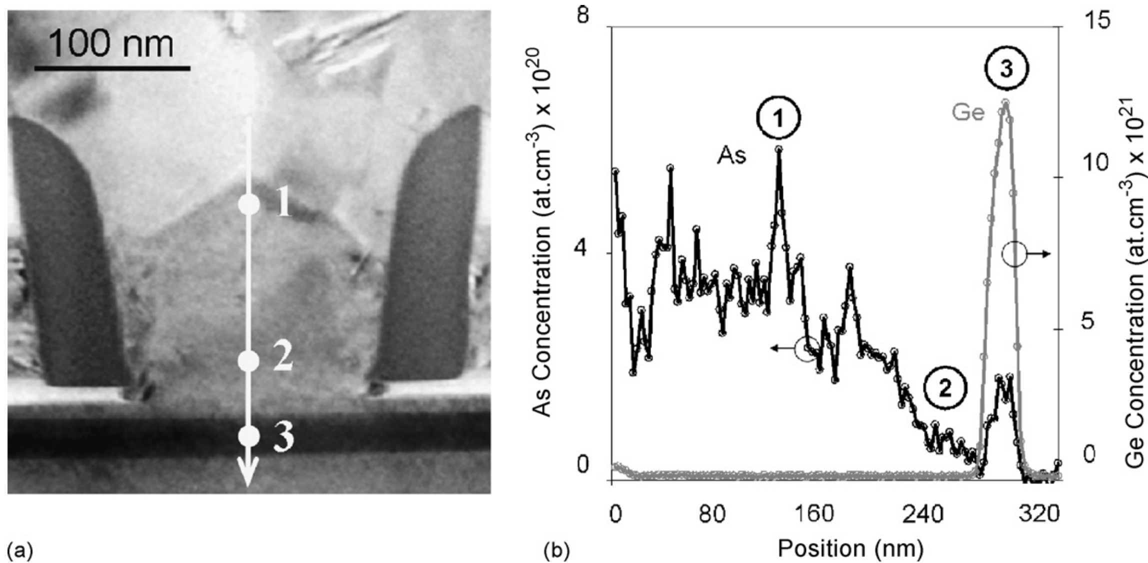

Fig. 12. (a) TEM image of the same HBT than in Fig. 11(a). The white arrow indicates the EDX profile and positions 1, 2 and 3 are reported on the following graph. (b) 120 keV STEM EDX profile acquire vertically along the HBT showing the As segregation at the grain boundaries (point 1) and the As depleted region (point 2) at the Ge base interface (point 3).

performed vertically across the BiCMOS are presented in Fig. 12. A high As concentration plateau in the top emitter region (around 3×10^{20} at. cm^{-3}) is observed. The EDX profile confirms the arsenic segregation at the grain boundaries (point 1). The As depleted region (point 2) is also shown near the bottom of the interface between the emitter and the base with a concentration about 5×10^{19} at. cm^{-3}, this corresponds to an arsenic detection of 0.1%. It has been clearly shown that this signal is detectable when comparing the undoped regions below the base.

6. Discussion

Nanoprobe STEM spectroscopy dopant analysis requires a high electron beam current. In this paper, we have not fully considered the radiation damage which will clearly exist for 200 keV electrons on silicon. This is out of the scope of this paper and will be the subject of a complete study in a future publication. However, EELS spectroscopy is a sensitive technique which gives good signal-to-noise ratio for low doses (see Fig. 4a). For this reason EELS analyses have been performed at 200 keV. On the contrary, EDX spectroscopy is not sensitive at low dose (see Fig. 2a) but, due to low background, the signal-to-noise ratio increases without saturation when the dose increases. This is why 120 keV was chosen in this work for EDX high dose analysis.

STEM EELS is proven to be a technique which can be very reliable and calibrated for quantification. On the contrary, for STEM EDX, some experimental parameters and phenomena induce erratic fluctuations of about ±30% (variable absorption depending on X-ray energy and sample thickness, channelling/diffraction effect in mono crystal, detector counting rates and dead times ...). The applications presented in this paper are encouraging for examining arsenic doping inside structures as small as 10 nm, especially when compared to the micrometer-scale structure needed for SIMS analysis. The As distribution and segregation in devices should be more frequently characterized in order to improve the knowledge of devices behaviour and simulation models.

7. Conclusion

Two-dimensional As dopant maps have been provided for real nm-scale devices with nanometer resolution using STEM EELS and EDX spectroscopies using a classical uncorrected FEG TEM. The sensitivity limit is found to be approximately 0.1%. Accurate quantification for STEM EELS has been demonstrated by comparison to a reference sample and SIMS analysis. Large structures have been compared to nanometer devices to verify the doping level variation. It is concluded that the doping level is the same but segregation at the initial epitaxy surface is different. Other devices analyzed (BiCMOS transistor) show heterogeneity in the distribution of arsenic with segregation at grain boundaries in poly silicon and at Si_3N_4 spacer surface. A depleted area near the emitter/base interface is observed due to the incorporation kinetics of arsenic in silicon during epitaxy.

Acknowledgement

The authors are grateful for the assistance of Dr. David Cooper.

References

Avenier, G., Chevalier, P., Troillard, G., Vandelle, B., Brossard, F., Depoyan, L., Buczko, M., Boret, S., Montusclat, S., Margain, A., Pruvost, S., Nicolson, S.T., Yau, K.H.K., Gloria, D., Dutartre, D., Voinigescu, S.P., Chantre, A., 2008. 0.13 μm SiGe BiCMOS technology for mm-wave applications.In: BCTM Proceedings. pp. 89–92.

Borot, G., Rubaldo, L., Clement, L., Pantel, R., Dutartre, D., Kuitunen, K., Slotte, J., Tuomisto, F., Mescot, X., Gri, M., Ghibaudo, G., 2007. Tensile strain in arsenic heavily doped Si. Journal of Applied Physics 102, 103505.

Carpenter, G.J.C., Phaneuf, M.W., Weaver, L., McCotter, D., 1999. Arsenic dopant profiling around trench capacitors in memory chip using EDX in a field emission TEM/STEM, 1999. In: Electron Microscopy and Analysis Group Conference. pp. 601–604.

Cliff, G., Lorimer, G.W., 1975. Journal of Microscopy 103, 203–207.

Cooper, D., Truche, R., Rivallin, P., Hartmann, J.M., Laugier, F., Bertin, F., Rouviere, J.L., Chabli, A., 2007. Medium resolution off-axis electron holography with millivolt sensitivity. Applied Physics Letters 91, 143501.

Delille, D., Pantel, R., Auvert, G., Van Cappellen, E., 1999. Thickness measurement of focused ion beam thinned silicon crystals using convergent beam electron diffraction and electron energy loss spectroscopy. In: Microscopy and Microanalysis, Proceedings. p. 898.

Eyben, P., Vandervorst, W., Alvarez, D., Xu, M., Fouchier, M., 2007. In: Kalinin, S., Gruverman, A. (Eds.), Probing Semiconductor Technology and Devices with Scanning Spreading Resistance Microscopy. Scanning Probe Microscopy. Springer, pp. 31–87.

Gault, B., Vurpillot, F., Vella, A., Gilbert, M., Menand, A., Blavette, D., Deconihout, B., 2006. Design of a femtosecond laser assisted tomographic atom probe. Review of Scientific Instruments 77, 043705.

Kelly, T.F., Miller, M.K., 2007. Invited review article: atom probe tomography. Review of Scientific Instruments 78, 031101.

Macaulay, J.M., Hull, R., Jalali, B., 1993. Characterization of arsenic doping profile across the polycrystalline Si/Si interface in polycrystalline Si emitter bipolar transistors. Applied Physics Letters 63, 1258–1260.

Parisini, A., Morandi, V., Solmi, S., Merli, P.G., Giubertoni, D., Bersani, M., van den Berg, J.A., 2008. Quantitative determination of the dopant distribution in Si ultrashallow junctions by tilted sample annular dark field scanning transmission electron microscopy. Applied Physics Letters 92, 261907.

Pei, L., Duscher, G., Steen, C., Pichler, P., Ryssel, H., Napolitani, E., De Salvador, D., Maria Piro, A.M., Terrasi, A., Severac, F., Cristiano, F., Ravichandran, K., Gupta, N., Windl, W., 2008. Detailed arsenic concentration profiles at Si/SiO_2 interfaces. Journal of Applied Physics 104, 043507.

Rau, W.D., Schwander, P., Baumann, F.H., Höppner, W., Ourmazd, A., 1999. Two-dimensional mapping of the electrostatic potential in transistors by electron holography. Physical Review Letters 82, 2614–2617.

Siegelin, F., Dubotzky, A., Danzfuss, B., Shomann, S., 2008. Dopant analysis on advanced CMOS technologies. In: Proceedings from the 34th International Symposium for testing and failure analysis.

Thompson, K., Flaitz, P.L., Ronsheim, P., Larson, D.J., Kelly, T.F., 2007. Imaging of arsenic cottrell atmospheres around silicon defects by three-dimensional atom probe tomography. Science 317, 1370–1374.

Topuria, T., James, E.M., Browning, N.D., 2001. Direct atomic scale characterization of interfaces and doping layers in field-effect transistors. Applied Physics Letters 79, 132–134.

Topuria, T., Browning, N.D., Ma, Z., 2003. Characterization of ultrathin dopant segregation layers in nanoscale metal-oxide-semiconductor field effect transistors using scanning transmission electron microscopy. Applied Physics Letters 83, 4432–4434.

Tsuneta, R., Koguchi, M., Nakamura, K., Nishida, A., 2002. A specimen-drift-free EDX mapping system in a STEM for observing two-dimensional profiles of low dose elements in fine semiconductor devices. Journal of Electron Microscopy 51, 167–171.

Wang, T.S., Cullis, A.G., Collart, E.J.H., Murrell, A.J., Foad, M.A., 2001. Profiling of low energy implanted As distributions in Si by using HAADF and EDX techniques in the transmission electron microscope. Microscopy of semiconducting materials. In: Proceedings of the Royal Microscopical Society Conference. pp. 357–362.